ELSEVIER

Contents lists available at ScienceDirect

## **Chemical Physics Impact**

journal homepage: www.sciencedirect.com/journal/chemical-physics-impact



## Full Length Article

# Novel silver vanadate coupled semiconductor nanocomposites for effective removal of toxic organics

S. Sasikruba<sup>a</sup>, R. Siranjeevi<sup>b</sup>, I. Muthuvel<sup>a,c</sup>, G. Thirunarayanan<sup>c</sup>, T. Rajachandrasekar<sup>a,\*</sup>

- <sup>a</sup> Photocatalysis Laboratory, Department of Chemistry, M.R. Govt. Arts College (Affiliated to Bharathidasan University, Tiruchirappalli-24), Mannargudi 614 001, Tamil Nadu, India
- b Department of Chemistry, Saveetha School of Engineering, Saveetha Institute of Medical and Technical Sciences, Saveetha University, Chennai 602 105, Tamil Nadu, India
- <sup>c</sup> Advanced Photocatalysis Laboratory, Department of Chemistry, Annamalai University, Annamalainagar 608 002, Tamil Nadu, India

#### ARTICLE INFO

#### Keywords: Photodegradation Ag<sub>3</sub>VO<sub>4</sub>/ZnO Wastewater treatment Acid Green-16 Acid Red-72

#### ABSTRACT

One of the world's most important challenges is the lack of access to clean water, and researchers are working tirelessly to find a solution. Nanotechnology-treated water is superior to conventionally treated water since it contains no hazardous microorganisms or organic dyes. In this study, the influence of light on  $Ag_3VO_4$  nanocomposites doped with synthesized ZnO nanoparticles was analyzed. SEM, FTIR, XRD, XPS, and UV–vis spectroscopy were just some of the methods used to characterize the as-prepared nanocomposites. An  $Ag_3VO_4$ /ZnO nanocomposite was used to successfully adsorb and photodegrade Acid Green-16(AG-16), and Acid Red-72(AR-72) from an aqueous solution. Visible light dramatically accelerates the adsorption and photodegradation of the  $Ag_3VO_4$ /ZnO nanocomposite compared to complete darkness. 77.52 %, 82.86 %, and 89.56 % of AG-16 and 77.11 %, 82.74 %, and 87.91 % of AR-72 were removed by the ZnO,  $Ag_3VO_4$ , and  $Ag_3VO_4$ /ZnO nanocomposites, respectively, in less than 60 min. However, visible-light photodegradation is more successful than adsorption alone in removing AG-16 and AR-72. In this pioneering study, we assess the catalytic performance of newly synthesized ZnO incorporated  $Ag_3VO_4$  nanocomposites for the UV-assisted degradation of organic dyes. Our study presents an innovative catalyst system that exhibits improved efficiency and holds promise for implementation in environmentally sustainable wastewater treatment methods.

## 1. Introduction

Most of the world's rivers, lakes, and seas are composed of water, which is a chemical liquid that is tasteless, odourless, and practically colourless. Water also makes up the majority of the fluids found within the bodies of most living creatures. Even though it does not contain any calories or organic nutrients, water is known as a universal solvent due to its capacity to dissolve a wide range of substances. This is despite the fact that water itself does not supply any of these things. Water is an essential component of all known forms of life [1]. The lack of access to clean water is already a big problem that is only expected to become worse in the years to come as a result of heavy global industrialization and rising human population [2]. The primary cause of pollution in the atmosphere is the introduction of unprocessed, raw waste into the environment [3]. This is accomplished mostly via the emissions produced by various forms of industrial activity. The discharge of untreated

or poorly treated effluent into the environment by industries results in the contamination of both the water and the soil. A high potential to cause cancer in people, as well as in animals and aquatic environments, and that they have a low rate of biodegradability [4]. In addition to this, it is neurotoxic, which means that it causes persistent damage to both animals and people. The dyes and pigments that are found in textile effluents may potentially contaminate water sources. The requirement for dyes for industrial uses is essential for society, despite the fact that they have an effect on the surrounding environment [5]. Because of its ease of use and modest power needs, adsorption is the most pragmatic method of pollution control currently available. The photocatalytic degradation of catalysts is an approach that seems to have more potential. The one tried-and-true strategy for enhancing the efficiency of degradation is to couple photocatalysts with photosensitizers or co-catalysts in order to form multi-component composite photocatalysts [6,7]. A potential photocatalyst is zinc oxide (ZnO), which has a higher

E-mail address: proftrchem1966@gmail.com (T. Rajachandrasekar).

<sup>\*</sup> Corresponding author.

photocatalytic effectiveness for the breakdown of organic contaminants [8].

In recent years, ZnO has become a lot of popularity, and it is now utilized in a wide variety of applications, such as solar cells, transparent conductive contacts, light-emitting devices, spintronic devices, laser deflectors, paints, antibacterial agents, biosensors, piezoelectric transducers, and gas sensors. ZnO is also used in a variety of paints, which are used to protect against bacteria. [9,10,11]. Recently, it was revealed that the small bandgap energy of silver vanadate (Ag<sub>3</sub>VO<sub>4</sub>), which is around 2.1 eV and significantly lower than that of silver halides, makes it a good candidate for visible-light-driven photocatalysis. This discovery was made possible by the fact that silver halides have substantially higher bandgap energies. After that, the nanocomposite was put through a series of tests to determine whether or not it has the capacity to eliminate Acid Green-16 dye from water when exposed to visible light. After 120 min of irradiation, the findings indicated that Ag<sub>3</sub>VO<sub>4</sub>/ZnO nanocomposite was very successful at removing the dye. The removal effectiveness of the nanocomposite was over 95 % after the dye was

The purpose of this investigation was to create one-of-a-kind  $Ag_3VO_4/ZnO$  hybrid photocatalysts with a range of  $Ag_3VO_4wt$ . Acid Green-16(AG-16) served as a model pollutant that was used in the experiment that investigated the photocatalytic activity of the  $Ag_3VO_4/ZnO$  nano combination when exposed to UV light. When compared to pure ZnO and  $Ag_3VO_4$ , the generated  $Ag_3VO_4/ZnO$  composites displayed remarkable photodegradation, photostability, and antibacterial activity [12]. This was achieved despite the removal of Acid Green-16 (AG-16). In this article, we discuss how the hydrothermal dispersion process may be used for the synthesis of oxide-wrapped ZnO silver vanadate. In addition, investigated whether or not  $Ag_3VO_4$  and ZnO are effective as catalysts for the breakdown of  $AG_1$ 0 and  $AR_2$ 1 when exposed to UV and solar irradiation [13].

The field of advanced nanomaterials for environmental remediation has seen a notable advancement with the creation of a novel nanocomposite known as Highly Visible Light Driven  $Ag_3VO_4/ZnO$ . The use of a new nanomaterial combining  $Ag_3VO_4$  and ZnO demonstrates the potential for a unique approach in effectively eliminating Acid Green-16 dye from aqueous solutions. This composite material harnesses the improved photocatalytic properties resulting from visible light, thereby presenting new opportunities in the pursuit of sustainable and efficient wastewater treatment. It effectively tackles a pressing environmental issue while also demonstrating the significant capabilities of nanotechnology in the realm of water purification.

#### 2. Materials and methods

### 2.1. Materials

Commercially accessible reagents, such as Acid Green-16 and Acid Red-72, Zinc nitrate hexahydrate, silver nitrate, oxalic acid dihydrate (Merck), ceric ammonium nitrate, and ammonium metavanadate (Qualigens), were used as provided. The experimental solution was prepared using double-distilled deionized water

#### 2.2. Synthesis of ZnO nanoparticles

The hydrothermal approach was used to synthesize ZnO nanoparticles. In a standard experimental procedure, a solution containing 0.6 M concentration of zinc nitrate was prepared by dissolving it in 100 ml of water. Subsequently, the resultant solution was carefully transferred into a separating funnel. A conical flask was used to administer a solution of oxalic acid at a concentration of 0.4 M The experimental procedure included the introduction of oxalic acid into a conical flask, followed by the addition of zinc nitrate into a separating funnel. The solution was agitated for a duration of two hours. The resultant solution, which exhibited a white appearance, was subjected to an aging process

lasting 2 h to facilitate gel formation. Subsequently, the solution was dried in a hot air oven at a temperature of 80 °C for a duration of 24 h The aerogel was subjected to calcination at temperatures of 400 °C, 500 °C, and 600 °C for a duration of 5 h to facilitate the production of ZnO nanoparticles. A solution containing one mole of ammonium metavandate was prepared by dissolving it in 35 ml of water. The solution was placed in a beaker and kept at a temperature of 80 °C using a magnetic stirrer. A solution containing two moles of silver nitrate was gradually introduced drop by drop into a separating funnel after its dissolution in 35 ml of water. Accordingly, a catalyst was synthesized.

#### 2.3. Synthesis of ZnO infused Ag<sub>3</sub>VO<sub>4</sub> nanocomposites

In a typical synthesis, 100 mL of 0.4 M zinc nitrate hexahydrate(A) and 100 mL of 0.6 M oxalic acid (B) were heated separately in deionized water, 100 mL of solution A was quickly added to solution B, 54 mg of  $Ag_3VO_4$  was previously synthesized, and the combined suspension was agitated for 3 h Filtered and repeatedly rinsed with DI water, the precipitated zinc oxalate dehydrates produced with  $Ag_3VO_4$  is then used. In a silica crucible, the  $Ag_3VO_4$ -zinc-zincate dehydrate-coupled system is heated in a muffle furnace at a rate of 20  $^{\circ}\text{C}$  per minute for 6 h After 12 h, after the furnace has cooled to room temperature, the  $Ag_3VO_4$ /ZnO catalyst is collected and put to use. 2 wt percent of coated  $Ag_3VO_4$  is included in this catalyst.

## 2.4. Characterization of Ag<sub>3</sub>VO<sub>4</sub>/ZnO nanocomposites

Morphological and elemental assessments of  $Ag_3VO_4/ZnO$  nanoparticles were analyzed using a field emission scanning electron microscope (FEI Quanta FEG200- FESEM) and Bruker's Energy Dispersive Spectroscopy (EDS). Using a Benchtop X-Ray Diffractometer with Cu-K at 0.15,405 Å in the Braggs angle range  $2\theta$  ( $10-80^{\circ}$ ). To determine the surface chemistry of the sample, XPS (X-ray photoelectron spectroscopy) was carried out using a PH15000 versa probe III. To learn more about their composition and how it affects their performance, scientists turned to FTIR spectroscopy (ATR diamond accessory of IR tracer 100 AH/Japan). Using a UV-visible spectrophotometer, the optical properties of the sample synthesis were examined at (UV 2100, Shimadzu).

#### 2.5. Photocatalytic degradation

Acid Green-16(AG-16) and Acid Red-72(AR-72) were used to examine the photocatalytic activity of ZnO, Ag<sub>3</sub>VO<sub>4</sub>, and Ag<sub>3</sub>VO<sub>4</sub>/ZnO nanocomposites. The following steps were taken to test the freshly synthesized materials for their photocatalytic potential: The adsorptiondesorption equilibrium between the dye molecules and the photocatalyst surface was determined by combining 20 mg of ZnO, Ag<sub>3</sub>VO<sub>4</sub>, and Ag<sub>3</sub>VO<sub>4</sub>/ZnO nanocomposites with 100 ml of 20 mg/L AG-16, and AR-72 in the dark using a magnet for 30 min. This was done to guarantee that the dye molecules were equally dispersed across the photocatalyst surface. The mixture was exposed to visible light from a 400-Watt Xenon lamp for the permitted 60 min to facilitate photocatalytic breakdown. In order to analyze the photocatalytic degradation process at 640 nm and 515 nm, we tracked the change in absorbance values of AG-16, and AR-72 every 10 min throughout the irradiation operation. The key active chemicals responsible for color deterioration were also investigated in a trapping experiment. The dye solution contained a variety of scavengers, each at a concentration of 5M Isopropyl alcohol (IPA), benzoquinone (BQ), and ethylenediaminetetraacetic acid disodium (EDTA-2Na) were some of the scavengers used. These compounds were included as hole, hydroxyl, and superoxide anion scavengers. Additionally, the method assessed the degree to which the color had changed. Total organic carbon (TOC) was analysed with a Shimadzu TOC-VCPH (Kyoto, Japan) analyser.

Degradation efficiency ( %) =  $\frac{Initial\ absorbance - Final\ absorbance}{Final\ absorbance}\ X\ 100$ 

#### 3. Results and discussion

#### 3.1. Morphological studies

The surface morphology of the ZnO/Ag<sub>3</sub>VO<sub>4</sub> photocatalyst was shown in Fig. 1 using pictures captured by a scanning electron microscope. Ag<sub>3</sub>VO<sub>4</sub>/ZnO was scanned using SEM, and the result was a smooth, uniformly large number of aggregated nanoparticles with an abnormal size of less than 27 nm (various software packages) between nanoparticles [14]. SEM was used in order to further investigate the surface morphology of the catalyst. Images of a sample consisting of 5 wt percent Ag<sub>3</sub>VO<sub>4</sub>/ZnO at four different magnifications are shown in the figures. At any magnification, the surface of the ZnO nanomaterial, which is represented by the black area, contains cylindrical Ag<sub>3</sub>VO<sub>4</sub> nanoparticles, which are represented by the white region. It is possible to confirm the existence of elements such as zinc, silver, vanadium, and oxygen by conducting an EDX study on a sample that was obtained from a specific location. The atomic weight percentages and elemental atomic percentages are shown in Fig. 1E. In addition, an elemental mapping method was used in order to demonstrate the presence of these constituents. The colorful areas are those that have high quantities of the metals zinc, silver, vanadium, and oxygen (Fig. 2).

#### 3.2. X-ray diffraction pattern

The X-ray diffraction pattern of the ZnO nanoparticles synthesized by the sol-gel technique is shown in Fig. 3. The material that was generated exhibited particles inside the nanoscale range, as shown by the observable widening of the XRD peaks. Through the examination of X-ray diffraction (XRD) patterns, we successfully determined the peak intensity, location, and width, together with the Full-Width at Half-Maximum (FWHM) data. The hexagonal wurtzite phase of ZnO, characterized by lattice constants a=b=0.324 nm and c=0.521 nm

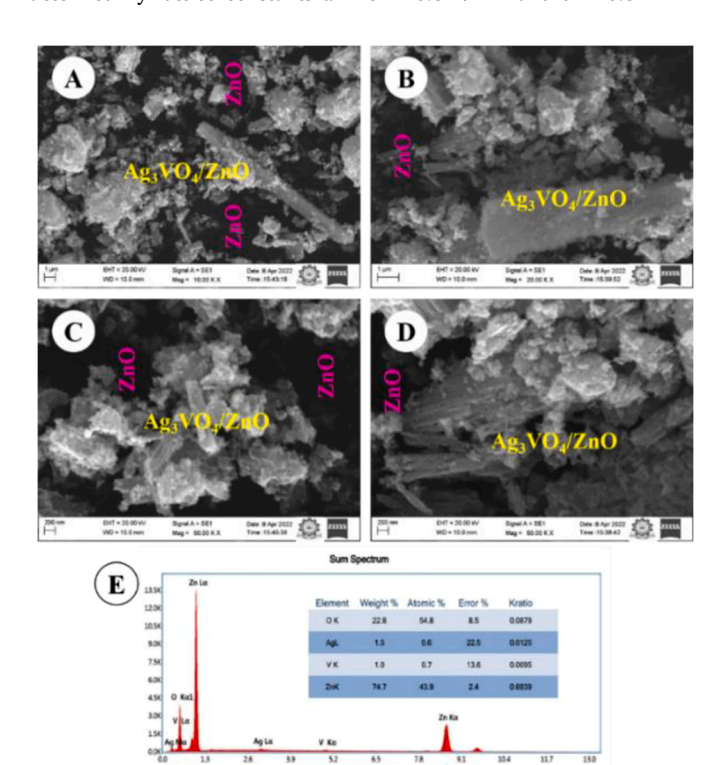


Fig. 1. SEM with EDS analysis of  $Ag_3VO_4/ZnO$  nanocomposites.

(JPCDS card number: 36–1451) [15], it has been meticulously documented in terms of its diffraction peaks at 31.84°, 34.52°, 36.33°, 47.63°, 56.71°, 62.96°, 68.13°, and 69° [15]. These peaks provide evidence for the presence of the hexagonal wurtzite crystal structure in ZnO and can be attributed to crystal planes (100), (002), (101), (102), (103), and (004) [16]. The (002) plane exhibited the most prominent diffraction peak, suggesting that ZnO nanorods (NRs) displayed a preference for development along the c-axis, which may be attributed to their comparatively greater surface energy [17]. Furthermore, the presence of the characteristic X-ray diffraction (XRD) peak of ZnO in the synthesized nanoparticles serves as evidence for the absence of any impurities. The diameter of the ZnO nanoparticles was calculated using the Debye-Scherrer formula [18].

$$D = \frac{0.9 \,\lambda}{\beta cos\theta} \,X\,100$$

Where, 0.89 is Scherrer's constant,  $\lambda$  is the wavelength of X-rays,  $\theta$  is the Bragg diffraction angle, and  $\beta$  is the full width at half-maximum (FWHM) of the diffraction peak corresponding to plane (101). The use of Scherrer's formula in relation to the full width at half maximum (FWHM) of the more prominent peak associated with the 101 planes, positioned at an angle of 36.33°, resulted in the determination of the average particle size of the examined sample as 16.21 nm. The evaluation of crystallite sizes was performed for the ZnO samples by using the most prominent peak of (101). The X-ray diffraction (XRD) patterns of Ag<sub>3</sub>VO<sub>4</sub>/ZnO and ZnO materials exhibited no discernible difference, indicating that the diffraction pattern of Ag<sub>3</sub>VO<sub>4</sub>/ZnO was identical to that of ZnO. Hence, it is evident that the  $Ag_3VO_4/ZnO$  composite exhibits the Wurtzite crystal structure of ZnO. Furthermore, it was noticed that there were no newly detected peaks for Ag<sub>3</sub>VO<sub>4</sub> in the Ag<sub>3</sub>VO<sub>4</sub>/ZnO catalyst. However, it was noted that Ag<sub>3</sub>VO4 exhibited more pronounced peaks at certain wavelengths, including 24.88°, 25.62°, 39.82°, 40.44°, 45.44°, 46.56°, 49.45°, 53.35°, 55.48°, 59.13°, and 60.28° (Fig. 1b). The observed absence of the  $Ag_3VO_4$  peak in  $Ag_3VO_4/ZnO$ could potentially be attributed to the relatively low concentration of Ag<sub>3</sub>VO<sub>4</sub> on the ZnO substrates.

## 3.3. FTIR spectra

ZnO, Ag<sub>3</sub>VO<sub>4</sub>, and Ag<sub>3</sub>VO<sub>4</sub>/ZnO are the products that were generated, and their FT-IR spectra are shown in Fig. 4. The OH stretching vibrations that were present in each and every sample were in the range of 3400 to 3450 cm<sup>-1</sup>. A significant vibration band with a frequency range of 400 to 500 cm<sup>-1</sup> was found to be the most effective way to illustrate the stretching mode of the Zn-O bond. This band is shown in Fig. 4A. The high absorption peak at 769 cm<sup>-1</sup> that is generated by VO<sub>4</sub>-3V-O bonding is shown in Fig. 4B. On the other hand, the weak absorption peak that is created by Ag-O bonding is displayed at 497 cm<sup>-1</sup>. It is determined that these two peaks represent strong absorption peaks and weak absorption peaks, respectively. A further discovery was made about the existence of shallow O—H water bending and stretching bands. It is [14] Additionally observed were the frequencies of 3423  ${\rm cm}^{-1}$ , 1625  ${\rm cm}^{-1}$ , and 1392  ${\rm cm}^{-1}$ , respectively, which were adsorbed on the surface of Ag<sub>3</sub>VO<sub>4</sub>. The numbers [18,19]. Stretching vibrations of the Zn-O, VO<sub>4</sub>, and Ag-O bonds were discovered in the frequency range of 925–470  ${\rm cm}^{-1}$  , as shown in Fig. 4C. This has been determined by the stretching vibrations. It was determined that the atoms of Ag<sub>3</sub>VO<sub>4</sub> were successfully incorporated into the crystal structure of ZnO [20].

## 3.4. XPS analysis

As can be seen in Fig. 5, the inclusion of  $Ag_3VO_4$  into the ZnO matrix was also confirmed by high-resolution XPS. The existence of  $Ag_3VO_4$  was established by the core-level spectra of Ag 3d in Fig. 3A, which displayed strong peaks of  $Ag^+$  at 367 and 373ev for Ag 3d<sub>5/2</sub> and Ag 3d<sub>3/2</sub>, respectively. Additionally, the spectra of V 2p shown in Fig. 3b indicated

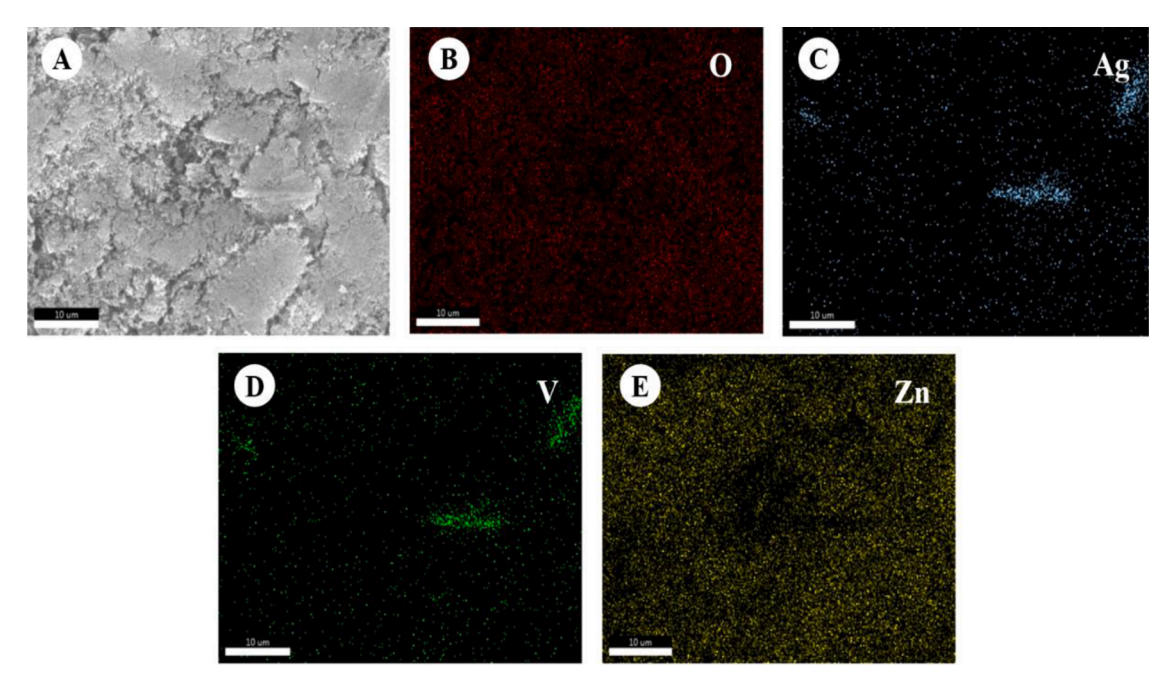


Fig. 2. Elemental color mapping images of Ag<sub>3</sub>VO<sub>4</sub>/ZnO nanocomposites.

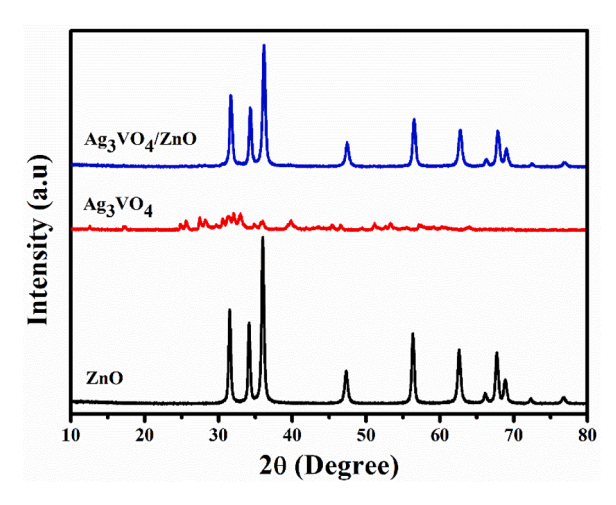


Fig. 3. XRD pattern of ZnO, Ag<sub>3</sub>VO<sub>4</sub>, and Ag<sub>3</sub>VO<sub>4</sub>/ZnO nanocomposites.

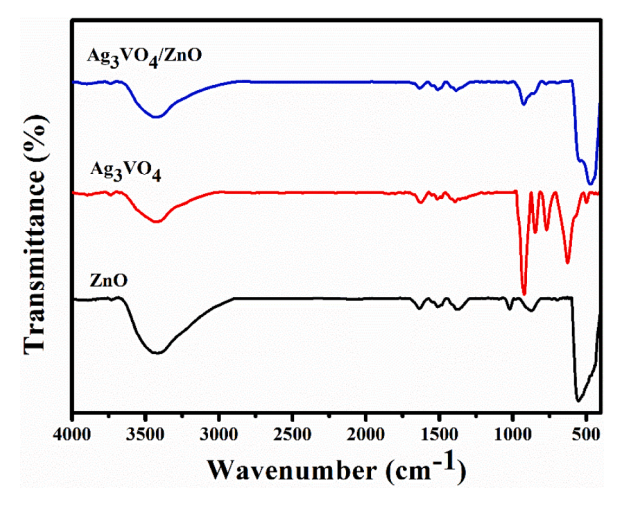


Fig. 4. FTIR spectrum of ZnO, Ag<sub>3</sub>VO<sub>4</sub>, and Ag<sub>3</sub>VO<sub>4</sub>/ZnO nanocomposites.

the oxidation number ( $^+$ 5) for the primary binding energies seen at 515 and 521ev. These energies specified the V  $2p_{3/2}$  and V  $2p_{1/2}$  orbits that were observed in heterojunctions that were identical to one another [21, 22]. Sharp XPS peaks of  $Zn^{2+}$  were found at 1022 and 1045ev for Zn  $2p_{3/2}$  and Zn  $2p_{1/2}$ , respectively, and are comparable to the wurtzite ZnO nanoparticles, as shown in Fig. 5E. In Fig. 5C of the O1s spectra, the lattice oxygen and the other adsorbed oxygen species were indicated at 518ev and 533ev, respectively [23]. As a result, the structural characterization of the triblock copolymer assisted sol-gel produced ZnO that was combined with coprecipitated  $Ag_3VO_4$  was carried out slowly.

## 3.5. UV-Visible spectroscopy

Fig. 6 displays the UV-visible spectra of ZnO as well as the composites of Ag<sub>3</sub>VO<sub>4</sub> and ZnO. The absorption spectrum of pure ZnO showed a distinct absorption edge at around 419 nm, but bulk Ag<sub>3</sub>VO<sub>4</sub> had a broader absorption range in the visible region, with an absorption edge located roughly 546 nm away. The spectrum absorption edges of Ag<sub>3</sub>VO<sub>4</sub>/ZnO composites are shown in Fig. 6, with corresponding values of 366 nm and 419 nm. A semiconductor with a narrow energy band gap, such as Ag<sub>3</sub>VO<sub>4</sub>, has the potential to cause a gradual increase in absorption in the visible spectrum. This would cause a shift towards longer wavelengths in the absorption edges. The introduction of Ag<sub>3</sub>VO<sub>4</sub> into ZnO resulted in a drop in the energy band gap from 3 eV to 2.5 eV, representing a reduction of 0.5 eV compared to ZnO. The Ag<sub>3</sub>VO<sub>4</sub>/ZnO composites exhibit a heightened level of visual absorption in comparison to pure ZnO. Indeed, the Ag<sub>3</sub>VO<sub>4</sub>/ZnO composites exhibit a higher level of visual absorption in comparison to Ag<sub>3</sub>VO<sub>4</sub> alone. The higher absorption in the visible region may be attributed to the production of an Ag<sub>3</sub>VO<sub>4</sub>/ZnO heterojunction. Furthermore, the absorbance increase observed may be attributed to the potential contribution of surface plasmon resonance (SPR) caused by Ag species derived from Ag<sub>3</sub>VO<sub>4</sub> [24,25].

## 3.6. Photodegradation studies

The photocatalytic performance of ZnO,  $Ag_3VO_4$ , and  $Ag_3VO_4$ /ZnO nanocomposites was analyzed under 500 W of Xenon lamp illumination using Acid Green-16(AG-16) and Acid Red-72(AR-72) as test chemicals. The degradation efficiency (AG-16 and AR-72) of the target dye on the

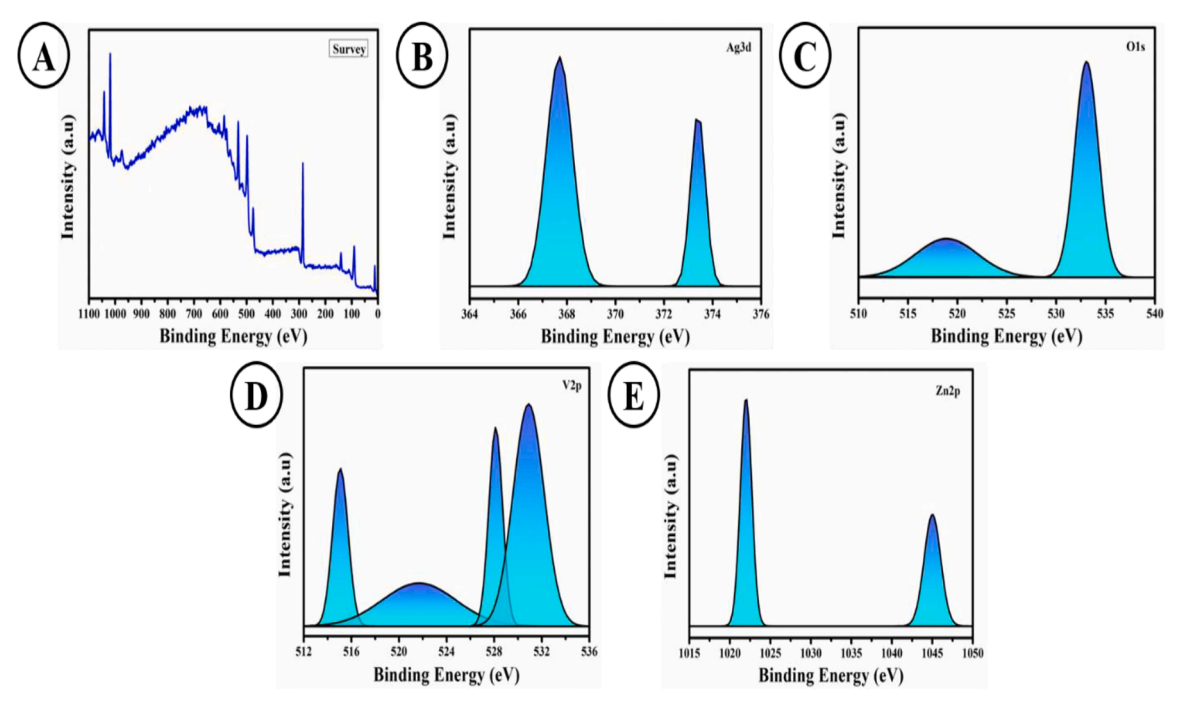


Fig. 5. XPS spectra of Ag<sub>3</sub>VO<sub>4</sub>/ZnO nanocomposites.

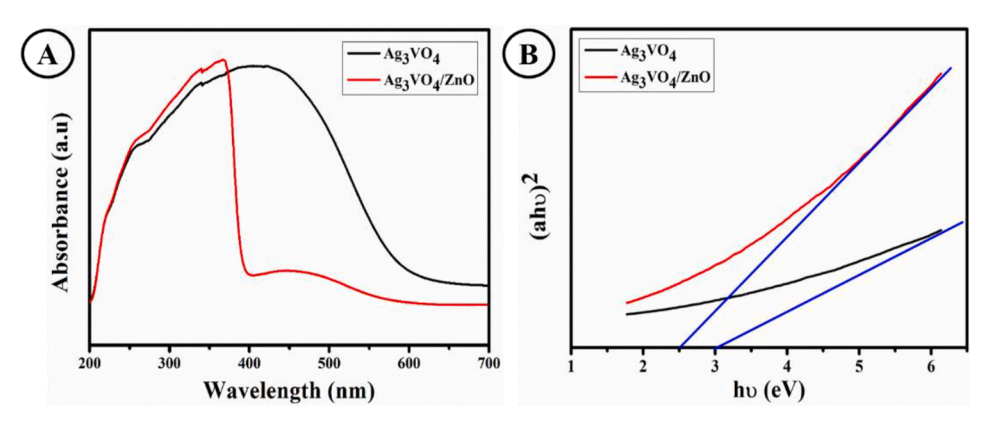


Fig. 6. UV-visible spectrum of  $Ag_3VO_4$  and  $Ag_3VO_4$ /ZnO nanocomposites.

newly manufactured photocatalysts changes with reaction time, as shown in Figures-7 and 8. These photocatalysts are currently in the production phase. Nanocomposite (ZnO, Ag<sub>3</sub>VO<sub>4</sub>, and Ag<sub>3</sub>VO<sub>4</sub>/ZnO) nanoparticles showed 41.31 %, 52.3 %, and 61.74 % degradation when exposed to a visible source for 20 min, while pure ZnO nanoparticles showed 41.19 %, 52.46 % degradation, and 61.26 % degradation. The color faded with time, as measured by a lessening of the absorption peak strength of the AG-16 and AR-72 dyes at various times. Since the absorption peak's strength decreased with time, it's possible that photodegradation of the dye is to blame for the color shift [26]. The experimental findings suggest that AG-16 and AR-72 are degraded more quickly by photocatalytic degradation in Ag<sub>3</sub>VO<sub>4</sub> and Ag<sub>3</sub>VO<sub>4</sub>/ZnO nanocomposites than in ZnO after 60 min of exposure to visible light. The assumption that Ag<sub>3</sub>VO<sub>4</sub> and Ag<sub>3</sub>VO<sub>4</sub>/ZnO nanocomposites are more stable than ZnO led to this finding.

This is shown by the fact that the absorption peak has almost disappeared entirely. In addition to this, it was found that the photo-degradation efficiency of AG-16 and AR-72 dyes was improved when ZnO was used as the catalyst. when being illuminated for 60 min,  $\rm Ag_3VO_4$  displayed (82.86 %) for AG-16 and (82.74 %) for AR-72, while the composite exhibited  $\rm Ag_3VO_4/ZnO$  (89.56 %) for AG-16 and (87.91

%) for AR-72. These results were obtained when the  $Ag_3VO_4$  was exposed to light. When measured against the rate of AG-16 decomposition, the rate of AG-16 degradation was significantly quicker. The study indicates that the photocatalytic activity of the  $Ag_3VO_4/ZnO$  nanocomposite under UV-visible irradiation is much higher than that of ZnO and  $Ag_3VO_4$  respectively. The comparison of the three different sets of data reveals this to be true. This was a result of the very simple design of AG-16 and AR-72. In addition to this, when employed by itself, AG-16 and AR-72 has the potential to function as a photocatalyst sensitizer. This behavior may have something to do with the presence of  $Ag_3VO_4$  on ZnO nanosheets, which promotes the separation of electrons and holes, as can be seen in Fig. 7 and Fig. 8(A). The statistics illustrate the probability of this occurring [27,28].

In order to study the degradation of AG-16 and AR-72, the ln ( $C_0/C_t$ ) versus time graphs were plotted for ZnO, Ag<sub>3</sub>VO<sub>4</sub> and Ag<sub>3</sub>VO<sub>4</sub>/ZnO nanocomposites. The observed rate constants for AG-16 degradation were k1=0.0248 min<sup>-1</sup>, K2=0.0263 min<sup>-1</sup>, and K3=0.0251 min<sup>-1</sup>, while for AR-72 degradation, the rate constants were k1=0.0245 min<sup>-1</sup>, K2=0.0262 min<sup>-1</sup>, and K2=0.0260 min<sup>-1</sup>, respectively [29]. These results indicate that the nanomaterials follow pseudo-first-order kinetics, as determined by the Langmuir-Hinshelwood model.

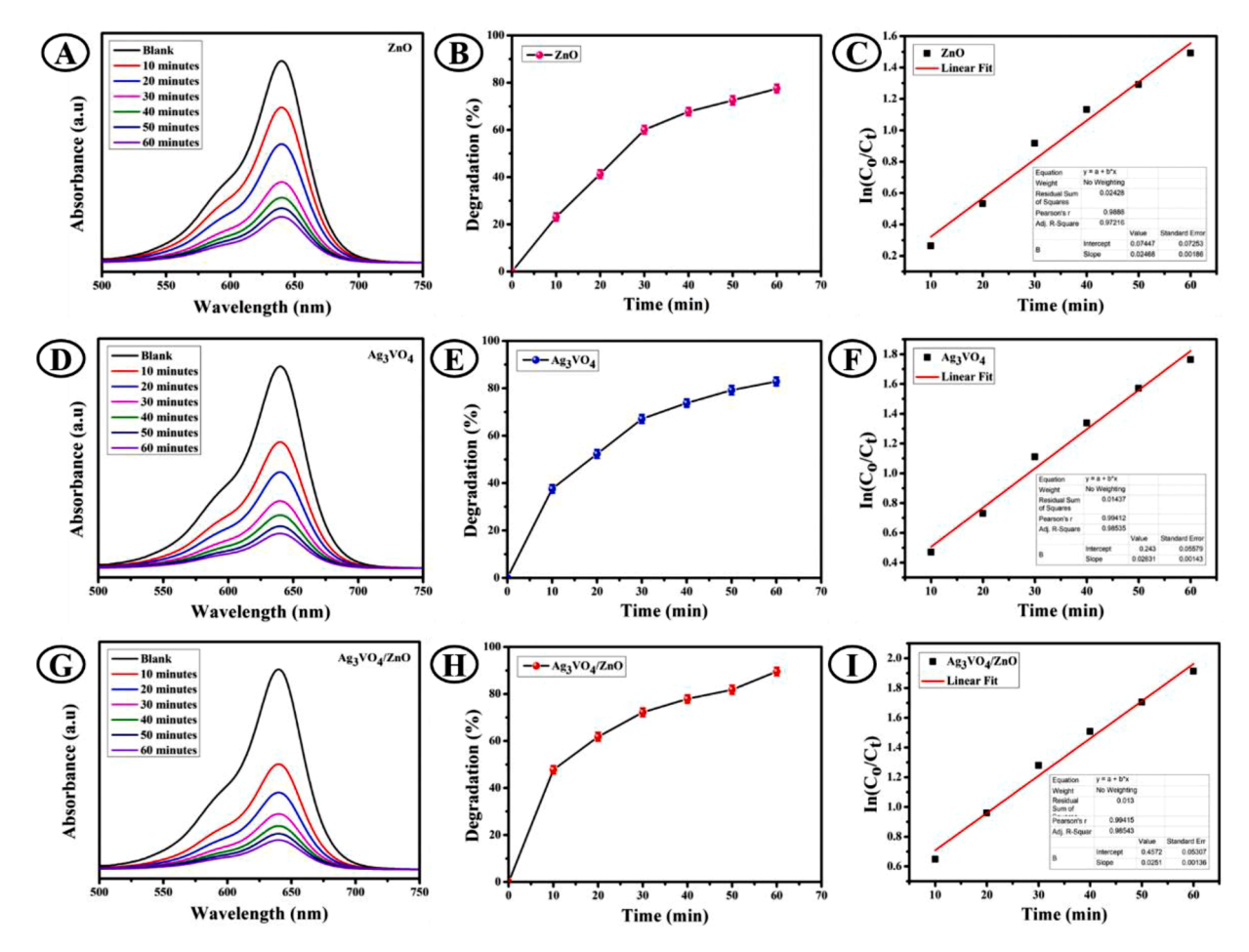


Fig. 7. Photodegradation studies of ZnO,  $Ag_3VO_4$ , and  $Ag_3VO_4$ /ZnO nanocomposites using Acid Green-16(AG-16). (For interpretation of the references to color in this figure legend, the reader is referred to the web version of this article.)

$$ln\frac{C_o}{C_t} = kt$$

The symbol 'k' stands for the pseudo-first-order rate constant for the photodegradation of AG-16 caused by AR-72 (min $^{-1}$ ). Regression values (R $^2$ ) for AG-16 on Ag $_3$ VO $_4$ /ZnO (0.9854) were much closer to one than for Ag $_3$ VO $_4$ (0.9941), and AR-72 on Ag $_3$ VO $_4$ /ZnO (0.9909) were much closer to one than for Ag $_3$ VO $_4$ (0.9861) which showed that first-order kinetics fit the nano-composite system better than Ag $_3$ VO $_4$ /ZnO nanoparticles [30].

The Ag<sub>3</sub>VO<sub>4</sub>/ZnO composite was shown to improve the photocatalytic degradation of AG -16 and AR-72 by the production of electron-hole pairs between the valence and conduction bands of Ag<sub>3</sub>VO<sub>4</sub>/ZnO. This process was triggered by the absorption of UV light by Ag<sub>3</sub>VO<sub>4</sub>/ZnO, as seen in Fig. 8. The photogeneration of electron-hole pairs between the valence (VB) and conduction (CB) bands of Ag<sub>3</sub>VO<sub>4</sub>/ ZnO was shown. The temporal uptake of AG-16 and AR-72 by Ag<sub>3</sub>VO<sub>4</sub>/ ZnO is shown below, measured in seconds. Moreover, the electrostatic interactions were responsible for the adsorption capacity of zinc oxide in the combined process of adsorption and photodegradation of AG-16 and AR-72 [31,32]. Reactant entrapment or reactant absorption is an additional property of aided photocatalysts that has been shown to enhance the transportation of reactants to active sites. This was shown by the observation that the photocatalysts that were supported had a significant inclination to either capture or absorb reactants [33]. The observed increase in photocatalytic activity in this study may have been attributed to a synergistic effect resulting from many causes. Several variables contributing to the performance of the Ag<sub>3</sub>VO<sub>4</sub>/ZnO nanocomposite include its high surface area, well-defined structure, efficient charge

carrier separation, outstanding electrical characteristics, and exceptional optical properties [34]. The following elucidation pertains to the proposed photocatalytic mechanism for nanocomposites:

$$Ag_3VO_4/ZnO + hv \rightarrow Ag_3VO_4/ZnO \left(e_{CB}^- + h_{VB}^+\right)$$
 (1)

$$Ag_3VO_4 + e_{CB}^- \rightarrow GO\left(e_{CB}^-\right)$$
 (2)

$$O_2 + ZnO\left(e_{CB}^-\right) \rightarrow O_2^{-} \tag{3}$$

$$O_2 + Ag_3VO_4(e_{CR}^-) \rightarrow O_2^-$$
 (4)

$$Ag_3VO_4/ZnO(h_{VB}^+) + (OH^-) \rightarrow Ag_3VO_4/ZnO + OH^-$$
 (5)

$$OH + Dyes \rightarrow Degradation products$$
 (6)

$$O_2^- + Dyes \rightarrow Degradation products$$
 (7)

The nanocomposite's behavior is superior to that of  $Ag_3VO_4/ZnO$  nanocomposites due to the graphene layers' capacity to decelerate the rearrangement process, as suggested by the theorized mechanisms. Moreover, the photocatalytic efficiency of an  $Ag_3VO_4/ZnO$  nanocomposite has the capacity to be enhanced due to its exceptional structure, high rate of charge carrier separation, expansive surface area, and outstanding optical and electrical properties of graphene layers. All of these contributing variables may account for the superiority of the graphene layers [35].

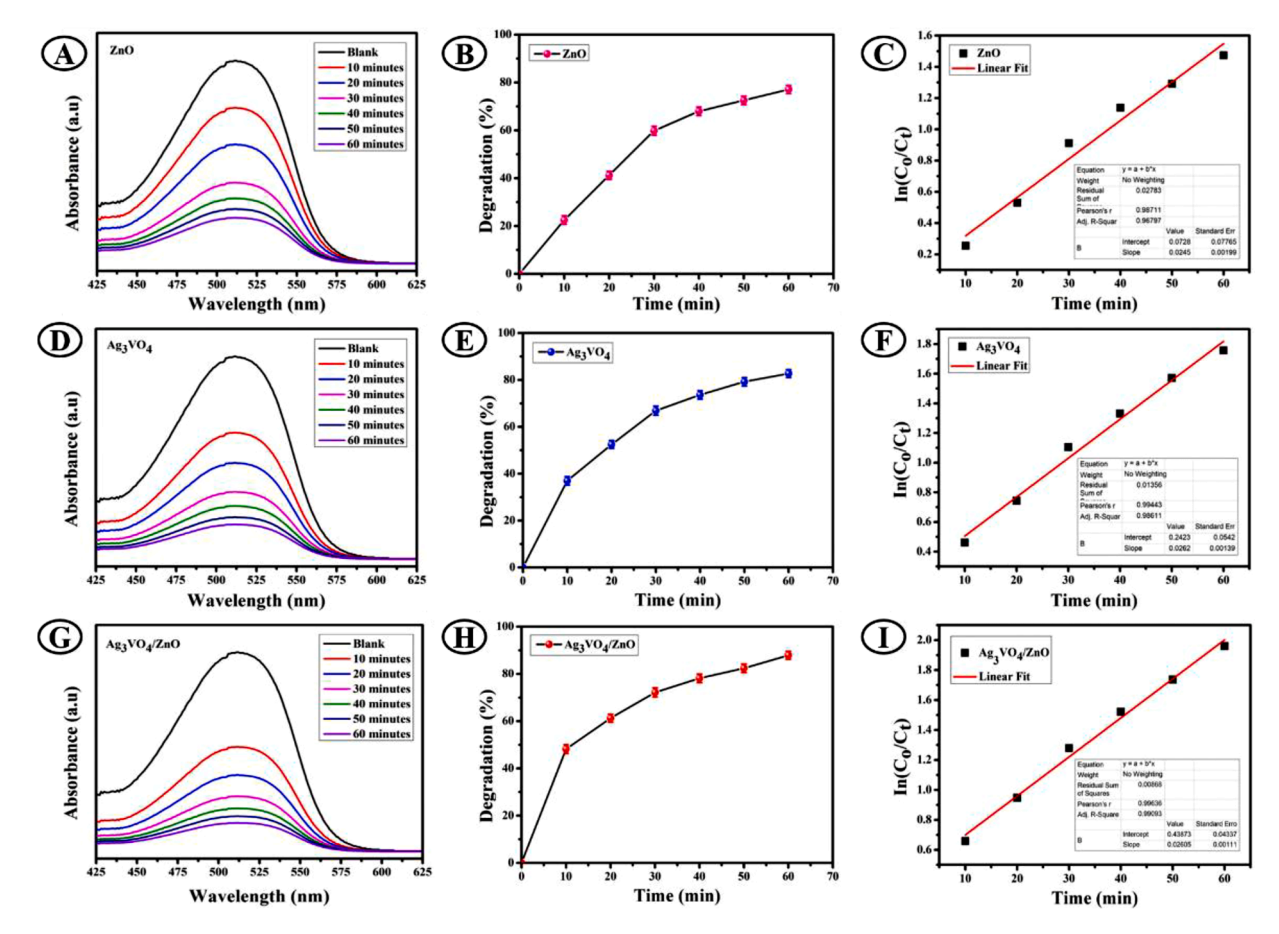


Fig. 8. Photodegradation studies of ZnO,  $Ag_3VO_4$ , and  $Ag_3VO_4$ /ZnO nanocomposites using Acid Red-72(AR-72). (For interpretation of the references to color in this figure legend, the reader is referred to the web version of this article.)

## 3.6.1. Radical entanglement

The researcher conducted experiments using photocatalysts and light sources, along with several radical scavengers including EDTA-2 Na as a hole-quencher (h<sup>+</sup>), to investigate the involvement of reactive oxidizing species in the degradation of AG-16 and AR-72 dyes. IPA effectively suppressed the hydroxyl radical ( $\bullet$ OH), but BQ effectively neutralized the superoxide radical anion ( $^{\bullet}$ O<sub>2</sub>). The quenchers infiltrated the photocatalyst system during its degradation. According to Fig. 10, the addition of BQ to the reaction vessel resulted in a degradation rate of 24.12 % for AG-16 and 25.62 % for AR-72. This exemplifies the significance of BQ in the decomposition of dye and highlights the involvement

of  $(^{\bullet}^-O_2)$  in this mechanism. Unlike  $(^{\bullet}OH)$  and  $(h^+)$ , the presence of EDTA-2 Na and IPA did not affect the degradation of the dye, suggesting that these ions had little effect on the photocatalytic activity [36] (Fig. 9) .

An experiment was conducted to assess the efficacy of removing AG-16 and AR-72 dyes. This was done by mixing 50 mL of a dye solution with 1 mL of isopropyl alcohol (IPA) in order to investigate the activation and impact of hydroxyl radicals ( $^{\circ}$ OH). Fig. 10 demonstrates a significant inhibition of photocatalytic studies with the introduction of alcohol (b)The Ag<sub>3</sub>VO<sub>4</sub>/ZnO catalysts produced maximum  $^{\circ}$ OH radical outputs of 65.34 % for AG-16 and 62.76 % for AR-72 after UV

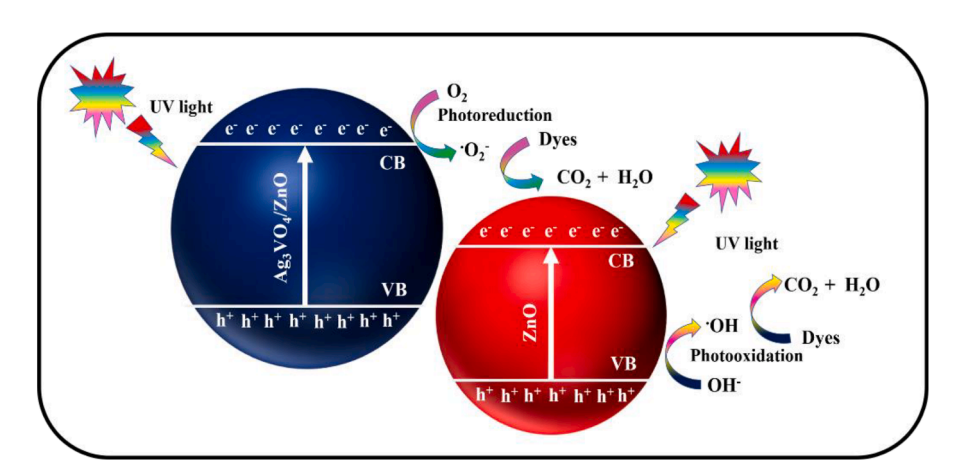


Fig. 9. Schematic mechanism of photocatalytic activity by ZnO and Ag<sub>3</sub>VO<sub>4</sub>/ZnO nanocomposite.

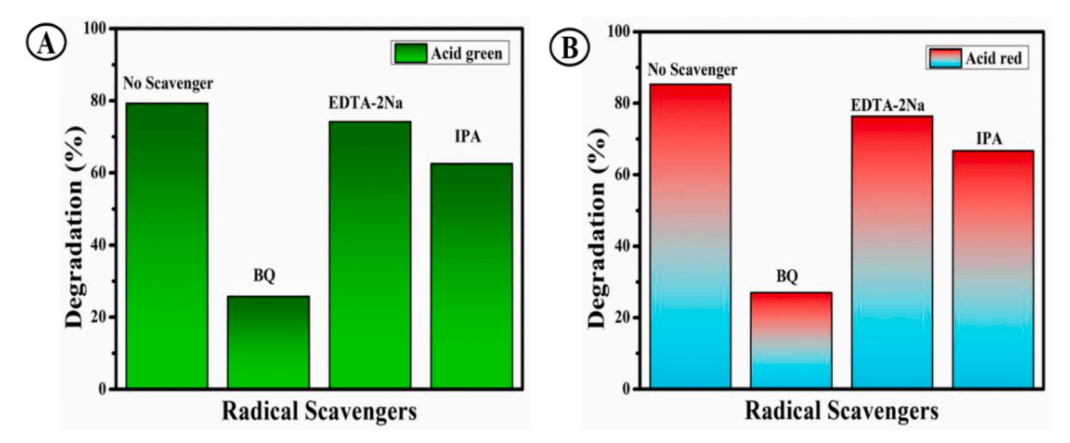


Fig. 10. Scavenger's studies on photocatalytic degradation of A). Acid Green-16(AG-16), and B). Acid Red-72(AR-72) over  $Ag_3VO_4/ZnO$  nanocomposite. (For interpretation of the references to color in this figure legend, the reader is referred to the web version of this article.)

irradiation. This study provides a comprehensive analysis of the very efficient scavenging of radicals by IPA, which occurs at an exceptionally fast rate. This process involves the consumption of \*OH radicals, as shown by Equation-8. The decolorization method of AG-16 and AR-72 dyes utilizes \*OH (Equation-9). However, the overall number of radicals produced in the medium and directly involved in contaminant oxidation can vary significantly due to various recombination processes between hydroxyl radicals (\*OH) and other radicals (Equation-10–12) [37].

Scavengers, including EDTA, were used to examine the formation and significance of photo-generated holes (h<sup>+</sup>) in photocatalytic study. With regards to Fig. 10. The efficiency of photocatalytic decolorization decreased from 100 % to 85.69 % for AG-16, and from 91.81 % to 85.69 % for AR-72, following the introduction of 5 mg of EDTA for a duration of 60 min. The following replies may provide insight on the findings: Two possible factors contribute to the significant decrease in bleaching effectiveness. Eqs. (13) and (14) illustrate that the holes (h+) first undergo reactions with H2O and OH, resulting in the production of a significant amount of hydroxyl radicals. Furthermore, the catalyst in an excited state has the ability to generate vacancies, which may then be used to directly oxidize the dye molecules according to Equation-15. Due to the consumption of holes by the first and second processes, the rate of rearrangements between electrons and holes is decreased. As a result, the half-lives of electrons are prolonged and reactive oxygen species (ROS) are generated at greater rates from electrons [38]. The effects of this phenomenon will be examined in the context of O2scavengers. The progressive incorporation of radicals onto the Ag<sub>3</sub>VO<sub>4</sub>/ZnO catalyst may be shown in Fig. 10.

The addition of 5 mg of benzoquinone to a 50 mL aqueous solution of dye significantly reduced the degradation rates of AG-16 and AR-72dyes.Within a span of 60 min, the elimination rates of dyes (AG-16 and AR-72) utilizing an Ag<sub>3</sub>VO<sub>4</sub>/ZnO catalyst reached zero while O<sub>2</sub>scavenging was taking place. In contrast, the removal efficiency of AG-16 employing a ZnO photocatalyst declined from 100 % to 20 % over the same duration. The superoxide radical is commonly acknowledged to have a pivotal function in the degradation of some pigments found in pollution. The process of electron/hole recombination may be decelerated by using the electrons generated by light, as shown in Equation-16. The following mechanisms, which result in the removal of O2- radicals and hydroxyl radicals from this source, provide a comprehensive explanation for the observed results. Initially, the superoxide radical anion may rapidly oxidize the contaminating molecule (Equation-17) or undergo a reaction with  $H^+$  to form the hydroperoxyl radical  ${}^{\bullet}$ OOH (Equation-18). The color molecules undergo oxidation in this process (Equation-19). Furthermore, the superoxide anion has the ability to generate H<sub>2</sub>O<sub>2</sub> and decompose it into hydroxyl radicals either directly (Equation-20) or indirectly (Equation-21) as described by (Equation-22)

and (Equation-23).

$$(CH_3)_2CHOH + HO \rightarrow (CH_3)_2CHO + H_2O$$
 (8)

$$HO + Dyes \rightarrow CO_2 + H_2O$$
 (9)

$$HO + HO \rightarrow H_2O_2$$
 (10)

$$O_2^{-} + HO^{-} \to OH^{-} + O_2$$
 (11)

$$OH^- + HO^- \rightarrow H_2O + O^-$$
 (12)

$$H_2O + h^+ \to HO^- + H^+$$
 (13)

$$h^+ + OH^- \rightarrow HO^- \tag{14}$$

$$Dyes + h^{+} \rightarrow Dyes^{+} \rightarrow Degraded water$$
 (15)

$$e_{(CB)}^- + (O_2)ads \to O_2^-$$
 (16)

Dyes + 
$$O_2^- \to CO_2 + H_2O$$
 (17)

$$H^+ + O_2^- \rightarrow HO_2 \tag{18}$$

$$Dyes + HO_2 \rightarrow CO_2 + H_2O \tag{19}$$

$$O_2^{-} + H_2O_2 \rightarrow HO^{-} + HO^{-} + O_2$$
 (20)

$$2H^+ + O_2^- + e_{(CB)}^- \to H_2O_2$$
 (21)

$$e_{(CB)}^- + H_2 O_2 \to 2HO$$
 (22)

$$H_2O_2 + h\nu \to 2HO \tag{23}$$

3.7. ZnO, Ag<sub>3</sub>VO<sub>4</sub>, and Ag<sub>3</sub>VO<sub>4</sub>/ZnO nanocomposites reusability and stability over degradation by photocatalysis of Acid Green-16(Ag-16) and Acid Red-72(Ar-72)

The study investigated the photocatalytic durability and recyclability of ZnO,  $Ag_3VO_4$ , and  $Ag_3VO_4/ZnO$  nanocomposites after three cycles of photocatalytic activity. The findings of three distinct cycles using ZnO,  $Ag_3VO_4$ , and  $Ag_3VO_4/ZnO$  nanocomposites are shown in Fig. 11. The data is presented as the ratio of removal efficiency (in percent) to reaction time (in minutes). Following each cycle, the catalyst may be retrieved for further use by the process of centrifugation, which involves separating the newly obtained colors from the catalyst and then precipitating them. The investigation revealed that nanocomposites consisting of ZnO,  $Ag_3VO_4$ , and  $Ag_3VO_4/ZnO$  exhibited excellent

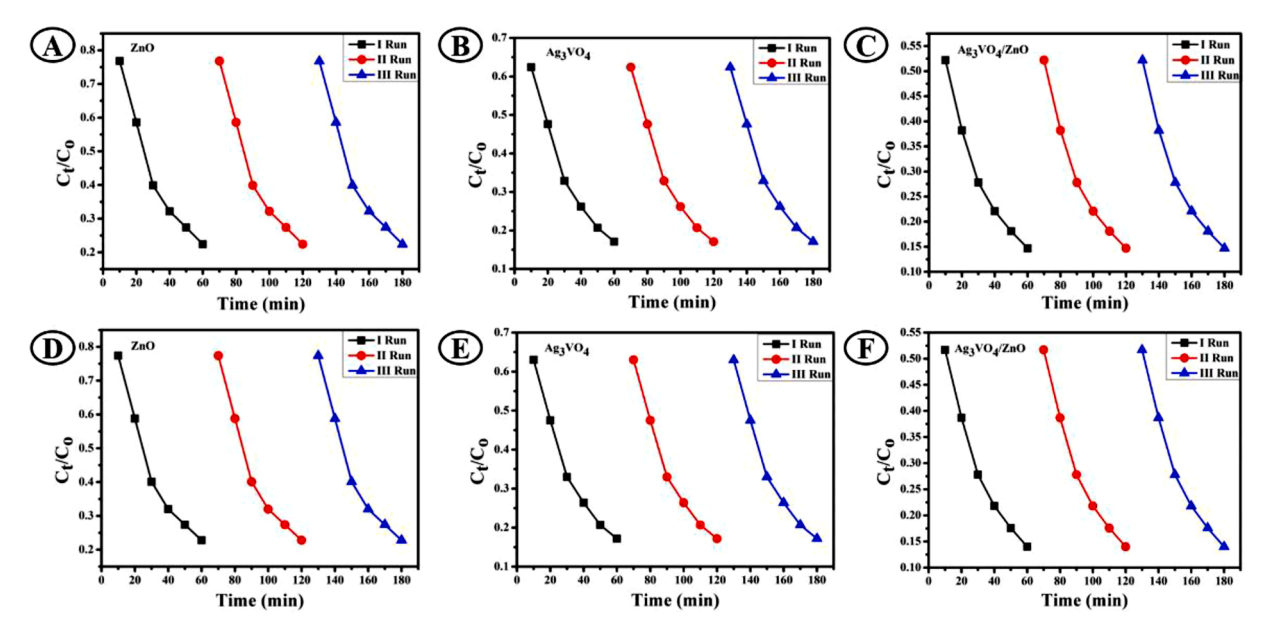


Fig. 11. Evaluation of the reusability of ZnO,  $Ag_3VO_4$ , and  $Ag_3VO_4$ /ZnO nanocomposites for photocatalytic degradation of A). Acid Green-16(AG-16), and B). Acid Red-72(AR-72). (For interpretation of the references to color in this figure legend, the reader is referred to the web version of this article.)

performance and were capable of several recyclings under visible light exposure. Fig. 11 demonstrates that the catalyst's efficiency might diminish by up to 10 % after being utilized three times. Following three cycles, there was no apparent reduction in the photocatalytic activity. The degradation rates of Acid Green-16(AG-16) and Acid Red-72(AR-72) dyes in ZnO, Ag<sub>3</sub>VO<sub>4</sub>, and Ag<sub>3</sub>VO<sub>4</sub>/ZnO nanocomposite were 84.96 %, 91.81 %, and 84.76 % respectively in the first run, 83.45 %, 89.62 %, and 82.61 % respectively in the second run, and 81.78 %, 87.66 %, and 80.92 % respectively in the third run. Furthermore, subsequent to the first test, it was discovered that an extended period of incubation was necessary to ensure the successful degradation of the dye [39,40]. The decrease in photocatalytic degradation studies seen after three cycles of reusability is likely due to overcrowding and/or a gradual decline in photocatalytic analysis efficiency [41-44]. These results further bolster the hypothesis that the technology might be used for wastewater treatment in environments that closely correspond to real-world environments [45-48].

## 3.8. Mineralization of dye

The total organic carbon (TOC) was measured in order to investigate the mineralization of Acid Green-16 (AR-16) and Acid Red (AR-72) in order to determine their respective mineralization. The removal of total organic carbon is illustrated in Fig. 12 by displaying how the breakdown

of AG-16 and AR-72 takes place when they are exposed to ultraviolet light. After being subjected to ultraviolet (UV) irradiation for a period of up to two hours, the total organic carbon (TOC) was shown to have seen an instantaneous drop. The mineralization of AG-16 and AR-72 occurred as a result of irradiation with a nanocomposite composed of  $Ag_3VO_4/ZnO$  for a period of five hours. The mineralization occurred at approximately 86.65 % and 89.82 % of total organic carbon reduction, respectively. The image shown in Fig. 13 was taken after the photosynthetic studies were completed. It is clear that this image has not undergone any morphological changes.

#### 4. Conclusion

In conclusion, the synthesized ZnO incorporated  $Ag_3VO_4$  nano-composites demonstrate promising catalytic activity for the UV-assisted degradation of Acid Green-16(AG-16) and Acid Red-72(AR-72), show-casing their potential as efficient catalysts in wastewater treatment applications. Further research is warranted to explore their broader environmental remediation applications. UV-visible spectroscopy was used in order to investigate the nucleation and development of ZnO,  $Ag_3VO_4$ , and  $Ag_3VO_4$ /ZnO nanocomposite. The absorption spectra of the process were consulted in order to ensure that these measurements were accurate. Scanning electron microscopy, often known as SEM, was used in this study so that the form and structure of nanoparticles could

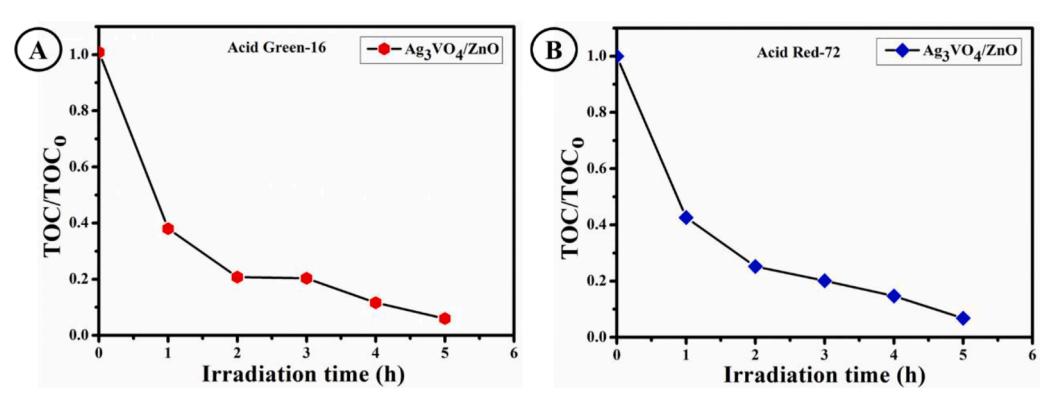


Fig. 12. Total Organic Carbon (TOC) of AG-16 and AR-72 during the photodegradation with Ag<sub>3</sub>VO<sub>4</sub>/ZnO nanocomposites using UV light.

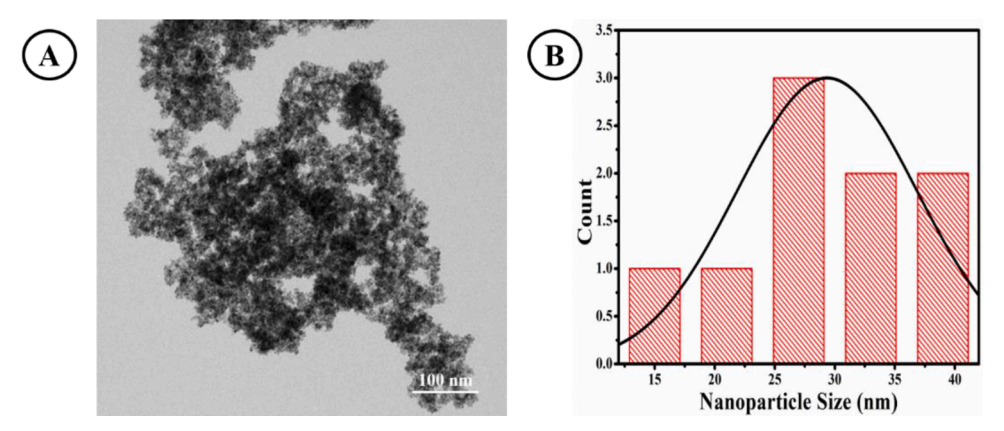


Fig. 13. After photodegradation studies HRTEM image of Ag<sub>3</sub>VO<sub>4</sub>/ZnO nanocomposites using UV light.

be analyzed. The biosynthesized ZnO, Ag<sub>3</sub>VO<sub>4</sub>, and Ag<sub>3</sub>VO<sub>4</sub>/ZnO nanocomposites all had crystal structures and particle sizes of around 16.37, 14.21, and 15.42 nm, respectively. Particle size and crystallinity were studied with the use of X-ray diffraction (XRD) peaks, which verified the biosynthesized crystal structures. This study revealed a viable method for the breakdown of Acid Green-16(AG-16) and Acid Red-72(AR-72). The research used biosynthesized ZnO, Ag<sub>3</sub>VO<sub>4</sub>, and Ag<sub>3</sub>VO<sub>4</sub>/ZnO nanocomposite. It also discussed the catalytic activity that gets rid of the dyes that are harmful to the environment. The first-order reaction kinetics was then followed by the photocatalytic performance against Acid Green-16(AG-16) and Acid Red-72(AR-72) dyes, both of which had a maximum degradation efficiency of 87.91 % and 89.56 %respectively. The Acid Green-16(AG-16), and Acid Red-72(AR-72) photocatalytic process that was created has the potential to replace the techniques that are currently used to treat Acid Green-16(AG-16), and Acid Red-72(AR-72). This is because the proposed process is superiorly simple, inexpensive, non-toxic, and recyclability, as well as stable, and output. This indicates that the proposed method for using photocatalysis in wastewater treatment may prove to be the approach that is most effective. The investigation into synthesized ZnO incorporated Ag<sub>3</sub>VO<sub>4</sub> nanocomposites as a catalyst for UV-assisted degradation of Acid Green-16(AG-16) and Acid Red-72(AR-72) has yielded groundbreaking insights. Our research reveals a novel and highly effective catalyst system that can significantly accelerate the degradation of these challenging organic dyes under UV irradiation. The synergistic interactions between ZnO and Ag<sub>3</sub>VO<sub>4</sub> in the nanocomposites have not only enhanced the catalytic activity but also demonstrated remarkable stability, highlighting their unique potential for sustainable and efficient wastewater treatment and pollution control. This novel catalyst system represents a significant advancement in the field of environmental remediation, with promising implications for addressing water pollution challenges.

#### CRediT authorship contribution statement

S. Sasikruba: Methodology, Formal analysis. R. Siranjeevi: Supervision, Investigation, Formal analysis. I. Muthuvel: Validation, Investigation, Formal analysis. G. Thirunarayanan: Writing – review & editing. T. Rajachandrasekar: Supervision, Methodology, Investigation.

## Declaration of competing interest

The authors declare that they have no known competing financial interests or personal relationships that could have appeared to influence the work reported in this paper.

#### Data availability

The data that has been used is confidential.

#### Acknowledgments

The authors are thankful to the Management of Saveetha School of Engineering, Saveetha University, Kattankulathur, Tamil Nadu, India for providing the facilities.

#### References

- [1] I. Muthuvel, B. Suwetha, T. Rajachandrasekar, S. Suguna, K. Gowthami, G. Thirunarayanan, T. Rajachandrasekar, Synthesis and characterization of carbon balls loaded silver orthophosphate for environmental remediation, J. Adv. Sci. Res. 12 (01 Suppl 1) (2021) 57–65.
- [2] M.A. Shanon, P.W. Bohn, M. Elimelech, J.G. Georgiadis, B.J. Marinas, M. Mayes, Nature 452 (2008) 301–310.
- [3] Z. Gao, S. Xie, B. Zhang, X. Qiu, F. Chen, Ultrathin Mg-Al layered double hydroxide prepared by ionothermal synthesis in a deep eutectic solvent for highly effective boronremoval, Chem. Eng. J. 319 (2017) 108–118, https://doi.org/10.1016/j. cei 2017/03/002
- [4] T. Chankhanittha, S. Nanan, Hydrothermal synthesis, characterization and enhanced photocatalytic performance of ZnO toward degradation of organic azo dye, Mater. Lett. 226 (2018) 79–82.
- [5] N.S. Sanjini, B. Winston, S Velmathi, Effect of precursors on the synthesis of CuO nanoparticles under microwave for photocatalytic activity towards methylene blue and rhodamine B dyes, J. Nanosci. Nanotechnol. 17 (1) (2017) 495–501.
- [6] X. Yu, J. Zhang, J. Zhang, J. Niu, J. Zhao, Y. Wei, B. Yao, Photocatalytic degradation of ciprofloxacin using Zn-doped Cu2O particles: analysis of degradation pathways and intermediates, Chem. Eng. J. 374 (2019) 316–327.
- [7] D. Yuan, L. Huang, Y. Li, H. Wang, X. Xu, C. Wang, L. Yang, A novel AgI/BiOI/pg-C3N4 composite with enhanced photocatalytic activity for removing methylene orange, tetracycline and E. coli, Dyes Pigm. 177 (2020) 108253.
- [8] D. Zheng, G. Wang, W. Huang, B. Wang, W. Ke, J.L. Logsdon, Z. Wang, W. Wang, J. Zhu, M. Yu, R. Wasielewski, M.G. Kanatzidis, T.J. Marks, A. Facchetti, Combustion synthesized zinc oxide electron-transport layers for efficient and stable perovskite solar cells, Adv. Funct. Mater. 29 (16) (2019) 1900265.
- [9] B. Macco, B.W. van de Loo, M. Dielen, D.G. Loeffen, B.B. van Pelt, N. Phung, J. Melskens, M.A. Verheijen, W.M. Kessels, Atomic-layer-deposited Al-doped zinc oxide as a passivating conductive contacting layer for n+-doped surfaces in silicon solar cells, Solar Energy Mater. Solar Cells 233 (2021) 111386.
- [10] A.A. Shah, M.A. Bhatti, A. Tahira, A.D. Chandio, I.A. Channa, A.G. Sahito, C. Ebrahim, M. Willander, N. Omer, Z.H. Ibupoto, Facile synthesis of copper doped ZnO nanorods for the efficient photo degradation of methylene blue and methyl orange, Ceram. Int. 46 (8) (2020) 9997–10005.
- [11] P.B. Chouke, A.K. Potbhare, G.S. Bhusari, S. Somkuwar, D. PMD Shaik, R. K. Mishra, R. Gomaji Chaudhary, Green fabrication of zinc oxide nanospheres by aspidopterys cordata for effective antioxidant and antibacterial activity, Adv. Mater. Lett. 10 (5) (2019) 355–360, https://doi.org/10.5185/amlett.2019.2235.
- [12] Z. Ying, X.F. Huang, X. Xiang, Y. Liu, X. Kang, Y. Song, S.Y. Chen, A safe and potent anti-CD19 CAR T cell therapy, Nat. Med. 25 (6) (2019) 947–953.
- [13] I. Muthuvel, K. Gowthami, G. Thirunarayanan, P. Suppuraj, B. Krishnakumar, A.J. F. do Nascimento Sobral, M. Swaminathan, Graphene oxide–Fe<sub>2</sub>V<sub>4</sub>O<sub>13</sub> hybrid material as highly efficient hetero-Fenton catalyst for degradation of methyl orange, Int. J. Ind. Chem. 10 (2019) 77–87.
- [14] S. Rajasri, S. Kalikeri, S. Balachandran, K. Gowthami, G. Thirunarayanan, M. Swaminathan, I. Muthuvel, Enhanced photodegradation of 2, 4-dinitrophenol by n-p type TiO<sub>2</sub>/BiOI nanocomposite, J. Indian Chem. Soc. 99 (3) (2022) 100337.

- [15] Z. Ayazi, F.S. Esfahlan, Z.M. Khoshhesab, ZnO nanoparticles doped polyamide nanocomposite coated on cellulose paper as a novel sorbent for ultrasound-assisted thin film microextraction of organophosphorous pesticides in aqueous samples, Anal. Methods 10 (25) (2018) 3043–3051. JCPDS, P. D. F. (1977). Alphabetical Index. Inorganic Compounds, International Centre for Diffraction Data, Newtown Square, Pa, USA.
- [16] M.A. Al-Belushi, M.T.Z. Myint, H.H. Kyaw, L. Al-Naamani, R. Al-Mamari, M. Al-Abri, S Dobretsov, ZnO nanorod-chitosan composite coatings with enhanced antifouling properties, Int. J. Biol. Macromol. 162 (2020) 1743–1751.
- [17] B.D. Cullity, Elements of X-ray Diffraction, Adison–Wesley Publ. Co., London, 1967.
- [18] A. Phuruangrat, P.O. Keereesaensuk, K. Karthik, P. Dumrongrojthanath, N. Ekthammathat, S. Thongtem, T Thongtem, Synthesis and characterization Ag nanoparticles supported on Bi<sub>2</sub>WO<sub>6</sub> nanoplates for enhanced visible-light-driven photocatalytic degradation of rhodamine B, J. Inorg. Organomet. Polym. Mater. 30 (4) (2020) 1033–1040.
- [19] G.J. Owens, R.K. Singh, F. Foroutan, M. Alqaysi, C.M. Han, C. Mahapatra, K. Hae-Won, J.C. Knowles, Sol-gel-based materials for biomedical applications, Prog. Mater. Sci. 77 (2016) 1–79.
- [20] P. Jansanthea, J. Kanthabangharn, W. Chomkitichai, J. Ketwaraporn, C. Saovakon, C. Wansao, W. Aimon, K. Parinya, P. Pusit, S.Phanichphant, Temperature-controlled synthesis and photocatalytic properties of ZnO–SnO<sub>2</sub> nanocomposites, J. Austr. Ceram. Soc. 57 (2) (2021) 579–588.
- [21] A. Suguna, S. Prabhu, R. Siranjeevi, S. Pugazhendhi, C. Sridevi, A detailed investigation on the structural, optical, and photocatalytic properties of ZnO@ZnS core-shell nanostructures, J. Mater. Sci. 34 (2023) 1655.
- [22] H. Li, W. Zhao, Y. Liu, Y. Liang, L. Ma, M. Zhu, C. Yi, L. Xiong, Y. Gao, High-level-Fe-doped P-type ZnO nanowire array/n-GaN film for ultraviolet-free white light-emitting diodes, Mater. Lett. 239 (2019) 45–47.
- [23] H. Yang, Q. Zhang, Y. Chen, Y. Huang, F. Yang, Z. Lu, Ultrasonic-microwave synthesis of ZnO/BiOBr functionalized cotton fabrics with antibacterial and photocatalytic properties, Carbohydr. Polym. 201 (2018) 162–171, https://doi. org/10.1016/j.carbpol.2018.08.068.
- [24] S.M. Mousavi, A.R. Mahjoub, R. Abazari, Facile green fabrication of nanostructural Ni-doped ZnO hollow sphere as an advanced photocatalytic material for dye degradation, J. Mol. Liq. 242 (2017) 512–519, https://doi.org/10.1016/j. mollig.2017.07.050.
- [25] X. Zeng, J. Yang, L. Shi, L. Li, M. Gao, Synthesis of multi-shelled ZnO hollow microspheres and their improved photocatalytic activity, Nanoscale Res. Lett. 9 (2014) 468, https://doi.org/10.1186/1556-276X-9-468.
- [26] Y. Qin, H. Li, J. Lu, Y. Yan, Z. Lu, X. Liu, Enhanced photocatalytic performance of MoS<sub>2</sub> modified by AgVO<sub>3</sub> from improved generation of reactive oxygen species, Chin. J. Catal. 39 (2018) 1470–1483, https://doi.org/10.1016/s1872-2067(18) 63111-0.
- [27] D. Liu, D. Chen, N. Li, et al., Integration of 3D macroscopic graphene aerogel with 0D-2D AgVO<sub>3</sub>·g·C<sub>3</sub>N<sub>4</sub> heterojunction for highly efficient photocatalytic oxidation of nitric oxide, Appl. Catal. B 243 (2019) 576–584, https://doi.org/10.1016/j. aprath 2018 11 012
- [28] R. Ran, X. Meng, Z. Zhang, Facile preparation of novel graphene oxide-modified Ag<sub>2</sub>O/Ag<sub>3</sub>VO<sub>4</sub>/AgVO<sub>3</sub> composites with high photocatalytic activities under visible light irradiation, Appl. Catal. B 196 (2016) 1–15, https://doi.org/10.1016/j. apcatb.2016.05.012.
- [29] Siranjeevi Ravichandran, Prakash Thangaraj, Prabhu Sengodan, Jeyalakshmi Radhakrishnan, Biomimetic facile synthesis of cerium oxide nanoparticles for enhanced degradation of textile wastewater and phytotoxicity evaluation, Inorg. Chem. Commun. 146 (2022) 110037, https://doi.org/10.1016/ i.inoche.2022.110037.
- [30] X.-J. Wen, C.-G. Niu, L. Zhang, C. Liang, H. Guo, G.-M. Zeng, Photocatalytic degradation of ciprofloxacin by a novel Z-scheme CeO<sub>2</sub>-Ag/AgBr photocatalyst: influencing factors, possible degradation pathways, and mechanism insight, J. Catal. 358 (2018) 141–154, https://doi.org/10.1016/j.jcat.2017.11.029.
  [31] C. Sun, Q. Xu, Y. Xie, Y. Ling, Y. Hou, Designed synthesis of anatase—TiO<sub>2</sub> (B)
- [31] C. Sun, Q. Xu, Y. Xie, Y. Ling, Y. Hou, Designed synthesis of anatase–TiO<sub>2</sub> (B) biphase nanowire/ZnO nanoparticle heterojunction for enhanced photocatalysis, J. Mater. Chem. A 6 (2018) 8289–8298, https://doi.org/10.1039/c7ta10274g.

- [32] M. Madkour, A.A. Ali, A. Abdel Nazeer, F. Al Sagheer, C. Belver, A novel natural sunlight active photocatalyst of CdS/SWCNT/CeO<sub>2</sub> heterostructure: in depth mechanistic insights for the catalyst reactivity and dye mineralization, Appl. Surf. Sci. (2020), https://doi.org/10.1016/j.apsusc.2019.143988.
- [33] Sasikala Velusamy, Karthik Palani, Ravichandran Siranjeevi, Prakash Natarajan, Mukkannan Azhagurajan, Rajesh Jegathalaprathaban, Effective removal of organic dyes using novel MnWO<sub>4</sub> incorporated CA/PCL nanocomposite membranes, Surf. Interfaces 40 (2023) 103008, https://doi.org/10.1016/j.surfin.2023.103008.
- [34] Z. Huang, K. Li, L. Yan, H. Guo, S. Luo, Fabrication of bio-based acidic nonmetals co-doped TiO<sub>2</sub> with core/shell structure and their unique photocatalytic performance for the rapid reduction of aqueous Cr(VI) under original pH and visible-light conditions, Appl. Catal. A 575 (2019) 142–151, https://doi.org/ 10.1016/j.apcata.2019.02.020.
- [35] Karthik Palani, Ravichandran Siranjeevi, Sasikala Velusamy, Prakash Natarajan, Mukkannan Azhagurajan, Rajesh Jegathalaprathaban, Effective photodegradation of organic water pollutants by the facile synthesis of Ag<sub>2</sub>O nanoparticles, Surf. Interfaces (2023) 103088, https://doi.org/10.1016/j.surfin.2023.103088.
- [36] K. Palani, R. Siranjeevi, S. Velusamy, M. Azhagurajan, R. Jegathalaprathaban, Evaluation of MnO<sub>2</sub> incorporated cellulose acetate membranes and their potential photocatalytic studies using Rhodamine-B dye, Process Saf. Environ. Protect. (2023), https://doi.org/10.1016/j.psep.2023.09.002.
- [37] S. Wang, Y. Guan, L. Wang, W. Zhao, H. He, J. Xiao, S. Yang, C. Sun, Fabrication of a novel bifunctional material of BiOI/Ag<sub>3</sub>VO<sub>4</sub> with high adsorption–photocatalysis for efficient treatment of dye wastewater, Appl. Catal. B 168–169 (2015) 448–457, https://doi.org/10.1016/j.apcatb.2014.12.047.
- [38] Ravichandran Siranjeevi, Sengodan Prabhu, Radhakrishnan Jeyalakshmi, Evaluation of biosynthesized nickel oxide nanoparticles from Clerodendrum phlomidis: a promising photocatalyst for methylene blue and acid blue dyes degradation, Ceram. Int. 49 (8) (2022) 12408–12414, https://doi.org/10.1016/j. ceramint.2022.12.100.
- [39] V. Sharma, P. Kumar, A. Kumar, K.A. Surbhi, K. Sachdev, High-performance radiation stable ZnO/Ag/ZnO multilayer transparent conductive electrode, Sol. Energy Mater. Sol. Cells 169 (2017) 122–131, https://doi.org/10.1016/j.sol mat.2017.05.009.
- [40] H. Dong, J. Li, M. Chen, et al., High-throughput production of ZnO-MoS<sub>2</sub>-graphene heterostructures for highly efficient photocatalytic hydrogen evolution, Materials (2019), https://doi.org/10.3390/ma12142233.
- [41] Siriwong Parada, Thongtem Titipun, Phuruangrat Anukorn, Thongtema Somchai, Hydrothermal synthesis, characterization, and optical properties of wolframite ZnWO<sub>4</sub> nanorods, CrystEngComm. 13 (2011) 1564–1569.
- [42] Pinchujit Soraya, Phuruangrat Anukorn, Wannapop Surangkana, Sakhon Thawatchai, Kuntalue Budsabong, Thongtem Titipun, Thongtem Somchai, Synthesis and characterization of heterostructure Pt/Bi<sub>2</sub>WO<sub>6</sub> nanocomposites with enhanced photodegradation efficiency induced by visible radiation, Solid. State Sci. 134 (2022) 107064.
- [43] Phuruangrat Anukorn, Wannapop Surangkana, Sakhon Thawatchai, Kuntalue Budsabong, Thongtem Titipun, Thongtem Somchai, Characterization and photocatalytic properties of BiVO4 synthesized by combustion method, J. Mol. Struct. 1274 (2) (2022) 134420.
- [44] Oranuch Yayapao, Titipun Thongtem, Anukorn Phuruangrat, Somchai Thongtem, Synthesis and characterization of highly efficient Gd doped ZnO photocatalyst irradiated with ultraviolet and visible radiations, Mater. Sci. Semicond. Process. 39 (2015) 786–792
- [45] H.B. Ahmed, Hossam E Emam, Seeded growth core-shell (Ag-Au-Pd) ternary nanostructure at room temperature for potential water treatment, Polym. Test. 89 (2020) 106720
- [46] H.E. Emam, Mary M. Mikhail, Samya El-Sherbiny, Khaled S. Nagy, Hanan B. Ahmed, Metal-dependent nano-catalysis in reduction of aromatic pollutants, Environ. Sci. Pollut. Res. 27 (2020) 6459–6475.
- [47] Hossam E. Emam, Hanan B. Ahmed, Reda M. Abdel hameed, Melt intercalation technique for synthesis of hetero-metallic@chitin bio-composite as recyclable catalyst for prothiofos hydrolysis, Carbohydr. Polym. 266 (2021) 118163.
- [48] Hanan B. Ahmed, Nourhan Saad, Hossam E. Emam, Recyclable palladium-based nano-catalytic laborer encaged within bio-granules for dye degradation, Surf. Interfaces. 25 (2021) 101175.